Journal of Materials Chemistry C

ROYAL SOCIETY OF CHEMISTRY

PAPER

View Article Online
View Journal | View Issue



Cite this: J. Mater. Chem. C, 2023, 11, 2619

# *In situ* photogenerated hydroxyl radicals in the reaction atmosphere for the accelerated crystallization of solution-processed functional metal oxide thin films†

Alicia Gómez-Lopez,‡ Y. Andrea Rivas, Sergio López-Fajardo, Ricardo Jiménez, Jesús Ricote, Carlos Pecharromán, Isabel Montero, Iñigo Bretos * and M. Lourdes Calzada *

We propose a disruptive method to process metal oxide thin films whereby hydroxyl radicals (•OH) are photogenerated *in situ* from the atmosphere where the corresponding solution-deposited layers are UV-irradiated. The reaction of these radicals with the film results in the transformation of the deposited layer into a highly-densified amorphous metal–oxygen network that easily evolves to the crystalline film at much lower temperatures than those traditionally used (over 600 °C). An exhaustive study has allowed us to determine the underlying mechanisms involved in the accelerated crystallization of these oxides by the presence of •OH radicals during the process. We demonstrate that the method is applicable to all-solution metal oxide thin films, validating its general application in thin films of the binary $Bi_2O_3$ oxide and of more complex oxides like $BiFeO_3$ and $Pb(Zr_{0.30}Ti_{0.70})O_3$ ferroelectric perovskites. It is shown that the metal oxide crystallization occurs between 250 °C and 350 °C, a temperature range hundreds of degrees below their conventional processing temperatures and fully compatible with their direct growth on flexible polymer substrates. This processing method opens new opportunities for the integration of high-performance multifunctional oxide layers into the next-generation devices demanded today by emerging technologies such as flexible or wearable electronics.

Received 21st December 2022,
Accepted 5th January 2023

DOI: 10.1039/d2tc05447g

rsc.li/materials-c



## 1. Introduction

Metal oxides have become essential for applications in thin film electronics or energy systems. Driven by the prospective development of the Internet of Things (IoT), the emerging technologies in the industry are demanding today the deposition of metal oxide thin films on cheap, lightweight and flexible substrates using sustainable fabrication processes with low-energy consumption and reduced carbon footprint.[1,2]

Among the methods employed to fabricate high-quality thin films, Chemical Solution Deposition (CSD) offers advantages over other techniques in terms of cost, scalability and deposition rate.[3] The preparation of metal oxide thin films from solutions typically involves the use of metal alkoxides and coordination complexes as chemical reagents, in which the metal cation (M) is bonded either to an alkoxy group (M–OR) or to an organic ligand (M–L). The formation of a metal–oxygen network (–M–O–M–) from the former precursors proceeds through the classical hydrolysis and condensation reactions of the sol–gel method. The process starts with the addition of water ($H_2O$) that reacts with the metal precursor through a nucleophilic substitution of the OR group by the hydroxyl groups (OH) of the water. Further condensation of the resulting products leads to the formation of metal–oxygen–metal chains, which is actually the building block of the metal oxide material (reaction (1)).

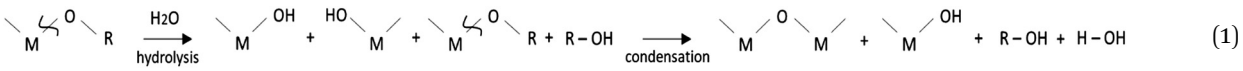


(1)

Unfortunately, the hydrolysis and condensation of metal alkoxides and coordination complexes usually occur simultaneously with a high reaction rate. They can result in an

*Instituto de Ciencia de Materiales de Madrid, Consejo Superior de Investigaciones Científicas (ICMM-CSIC). C/Sor Juana Inés de la Cruz, 3. Cantoblanco, 28049 Madrid, Spain. E-mail: ibretos@icmm.csic.es, lcalzada@icmm.csic.es*

† Electronic supplementary information (ESI) available. See DOI: https://doi.org/10.1039/d2tc05447g

‡ Present address: Instituto de Catálisis y Petreoquímica (ICP-CSIC). C/Marie Curie, 2. Cantoblanco. 28049 Madrid, Spain.

accelerated and uncontrolled gelation (even precipitation) of the solution that makes its subsequent deposition on a substrate not feasible. However, this issue can turn into a challenging opportunity if hydrolysis and condensation reactions take place in the deposited layer instead of in the precursor solution. Thus, the arrangement of the interconnected metal–oxygen network would be directly promoted in the film after the polycondensation among the different metal precursors. This could accelerate the early-stage formation of an amorphous oxide in the system under thermal conditions close to room temperature.

Applications such as thin film transistors or gate dielectrics using amorphous semiconductors require highly-densified transition metal oxide layers. Compaction and densification of the amorphous metal–oxygen network inevitably need an activation step by applying a moderate temperature (200–300 °C). However, crystalline layers are essential when other relevant functionalities such as piezoelectricity, ferroelectricity or superconductivity are intended to be used.[4–7] Here, the properties are linked to an ordered metal oxide structure and therefore, film crystallization demands higher annealing temperatures (usually over 600 °C) than those needed for just achieving film densification. This thermal treatment not only increases the complexity of the process, together with the economic and environmental load associated with the energy consumption, but also limits the choice of the substrate. For example, the low degradation temperature ($\leq$400 °C) of substrates based on plastic, textile or paper generally hinders the use of crystalline oxide films in emerging technologies such as flexible, wearable or foldable electronics.

Many researchers have recently developed new low-temperature solution processes particularly focused on the fabrication of amorphous metal oxide semiconductors. Among them, intriguing strategies based on a precise control of the reactions of hydrolysis and condensation (reaction (1)) produced during the formation of the metal–oxygen network are reported. Banger *et al.*[8] found that the presence of moisture during the heat treatment of solution deposited layers stimulates the hydrolysis and condensation reactions, leading to a reduced annealing temperature for amorphous In–Ga–Zn–O (IGZO) semiconductor thin films. Park *et al.*[9] made use of reactive radicals ($^{\bullet}NO_2$) formed after the photocleavage of solution layers containing nitrate salts. These radicals activated the polycondensation and densification of amorphous In–Zn–O (IZO) thin film transistors at moderate temperatures. Lee *et al.*[10] introduced hydrogen peroxide ($H_2O_2$) loading as an oxidizing agent during the formulation of $La_xZr_yO_z$ (LZO) precursor solutions. The combination of $H_2O_2$ and UV-irradiation in the spin-cast samples made possible the preparation of amorphous LZO films directly on polyimide substrates. While the aforementioned works are aimed at the formation of an amorphous metal–oxygen network in the material, not many papers have achieved the crystallization of solution-derived oxide layers at low temperatures. For example, Jao *et al.*[11] added organo-ammonium hydroxide salts into NiO precursor solutions to assure the presence of hydroxyl anions ($OH^-$) in the deposited layer. These anions accelerated the hydrolysis and condensation reactions that led to a reduction in the time and temperature to attain an incipient crystallization in the corresponding single-oxide film. In a rather distant field, Feng *et al.*[12] demonstrated that the crystallization of zeolites can be speeded up under hydrothermal conditions by inducing the polymerization of the aluminosilicate anions around the hydrated cations with UV-generated radicals. Therefore, some of the former works already show the significance that photochemistry has gained in the last years in the low-temperature processing of metal oxide thin films.[13]

Energy is always required to break the chemical bonds of molecules. If this energy is provided by light, it interacts with the bonding electrons of the chemical species triggering the decomposition of metal precursors. As photons with the proper wavelength have a very large quantum efficiency to be absorbed, the generated heat associated to the chemical reaction is nearly negligible, so that the whole process will take place at low temperatures. Thus, molecules can be cleaved by light into smaller molecules, individual atoms or reactive radicals. These species can further assist to the elimination of organic residuals, besides promoting the condensation and densification of the amorphous metal–oxygen network and even increasing the crystallization rate of the amorphous system. Whereas photochemical reactions have been traditionally induced in the thin film material, they can also take place in the irradiation atmosphere. Here, the primary process is the photolysis of gas molecules into reactive free radicals. This is usually followed by secondary processes that involve the attack of these radicals to the molecules of the gas, forming new radicals and molecular species. All these reactive compounds obtained from the irradiation atmosphere can react then with the thin film material and contribute to accelerate the crystallization of the metal oxide.

In this work, we propose a novel photochemical strategy to generate very reactive $^{\bullet}OH$ radicals within the atmosphere in which solution-deposited films are UV-irradiated. These species can react with the film surface through the substitution of the groups bonded to the metal (M–OR or M–L), playing the same role as that of the OH groups in the so-called hydrolysis reactions. However, the much higher reactivity of the $^{\bullet}OH$ radicals is able to trigger rapid and controlled reactions of nucleophilic substitution and condensation among precursors, enhancing (i) the formation of a highly-densified and defect-free amorphous metal–oxygen network and (ii) its subsequent crystallization into the metal oxide at very low temperatures. This strategy is demonstrated for high-*k* metal oxide thin films, particularly for multifunctional ferroelectric oxides (those dielectrics with the highest values of dielectric constant). These materials are one of the most demanding family of metal oxides, since not only a non-centrosymmetric crystal structure is required to support their functionality, but also several microstructural characteristics (*e.g.*, grain size, connectivity, *etc.*) are needed for achieving an adequate performance at low temperatures (see Table S1, ESI† that summarizes the properties of high-*k* dielectric films processed from solution at temperatures $\leq$400 °C).[1,9,14–42] Ferroelectric thin films provide besides a wide range of electrical properties (ferro-, pyro-,

 

piezoelectricity) that make them excellent candidates for their use in multifunctional electronic devices of emerging technologies. Finally, this low-temperature solution deposition method assisted by hydroxyl radicals can be applicable to the fabrication of metal oxide thin films of different compositions with either an amorphous or crystalline structure. This fact provides new opportunities for the integration of high-performance functional materials into next-generation devices (*e.g.*, flexible or stretchable electronic systems) using a low-cost, high-throughput and large-area deposition technique.

## 2. Results and discussion

Fig. 1 shows the scheme of the chemical solution deposition process devised in this work for accelerating the crystallization of metal oxide thin films. The synthesis of the metal oxide precursor solutions was carried out following the synthetic routes depicted elsewhere (Fig. S1, ESI†). Two continuous UV excimer lamps with wavelenghts of 172 and 222 nm were used to generate different irradiation atmospheres and to photoactivate the films along the different steps of the fabrication process (Fig. S2, ESI†). These UV sources have not enough power to significantly heat the irradiated material (thermal excitation), so that they result optimum for large-area coating and mass production scalability. The atmospheres introduced in the irradiation chamber were intentionally chosen for inducing the formation of reactive species in the gas medium (Fig. S3, ESI†). These species can react with the deposited layer leading to structural changes in the thin film material. The objective here is that all these photochemical reactions push the chemical system far away from equilibrium, thus accelerating processes that in principle can only be activated with thermal treatments at high temperatures.[12,13,43,44] According to the schematic drawing of Fig. 1, precursor solutions were deposited on rigid silicon substrates and dried at a low temperature ($\leq$150 °C). This results in gel layers that contain the metal precursors, organic solvents and pores occluded in a solid matrix (step 1 in Fig. 1(a)). The dried layers were then irradiated at 150 °C with light of 172 nm in an oxygen ($O_2$) atmosphere saturated with water ($H_2O$) vapor (step 2 in Fig. 1). Under this irradiation, the photolysis of the oxygen molecules present in the irradiation atmosphere produces free oxygen radicals ($O^\bullet$) that react with the water vapor, leading, in a primary process, to the formation of free hydroxyl radicals ($^\bullet OH$), (reaction (2) and (3), respectively).

$$O_2 \xrightarrow{h\nu} 2O^\bullet \quad (2)$$

$$O^\bullet + H_2O \rightarrow 2^\bullet OH \quad (3)$$

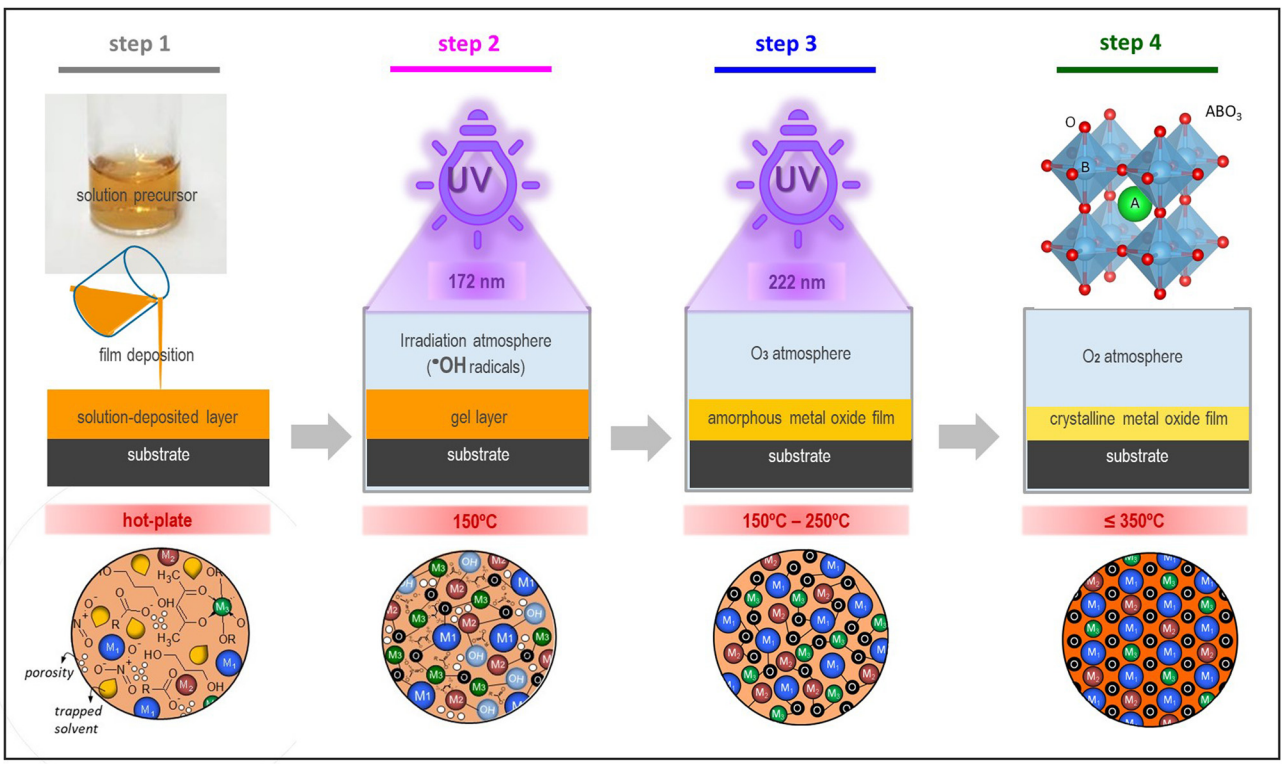


Fig. 1 Hydroxyl free radicals method for accelerating the formation and crystallization of solution-processed functional metal oxide thin films. The scheme shows the different steps of this method: solution deposition of the film onto the substrate (step 1), UV-irradiation of the deposited layer at $\lambda$ = 172 nm in a $^\bullet OH$ atmosphere (step 2), UV-irradiation of the film resulting from the step 2 at $\lambda$ = 222 nm in an $O_3$ atmosphere (step 3), and low-temperature treatment at temperatures $\leq$350 °C to attain the crystalline film (step 4). The drawings representing the characteristics of the films obtained after the different steps of the devised process are shown at the bottom. These drawings have been adapted with permission[4] from the Royal Society of Chemistry.

In this work, we propose that the •OH radicals formed in the irradiation atmosphere during this step will attack the gel layer and react with the chemical compounds contained in it,[12,43,44] accelerating the rate of the nucleophilic substitution of the OR groups and organic ligands by the •OH radicals and promoting the condensation among metal precursors (reaction (4) and (5), respectively).

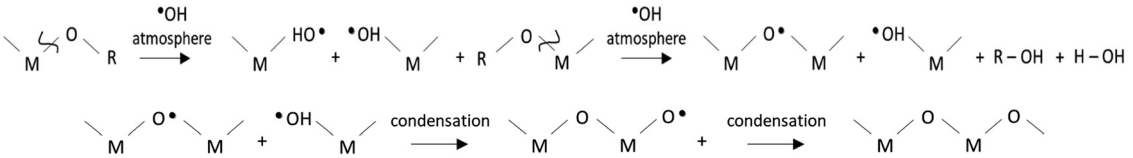


(4)

(5)

The byproducts of these reactions are mainly alcohols and water, which is therefore regenerated in the reaction media acting thus as a catalyst during the process and contributing to the formation of new •OH radicals in the irradiation atmosphere. In spite of the high yields of condensation obtained in the system during this step, the films were also subjected to a second UV exposure at 222 nm in a pure oxygen atmosphere and under heating at 250 °C (step 3 in Fig. 1(a)). This assures, on the one hand, the electronic photoactivation of the metal complexes contained in the film with absorption maxima close to the emission of this UV-lamp (Fig. 1(c) and Fig. S1c, ESI†).[34,35] On the other hand, the ozone ($O_3$) formed from the $O_2$ atmosphere under irradiation (reaction (6) and (7)), which can also occur as a secondary process at the step 2, produces a rapid elimination of molecular byproducts, organic residuals and voids remaining in the system (reaction (8)). This will increase the compaction of the solid metal–oxygen matrix resulting in an amorphous metal oxide film with a high degree of densification and a low content of defects.[13] As a consequence, the system can evolve to the crystalline phase by just applying a thermal treatment at such a low temperature of $\leq$350 °C (step 4 in Fig. 1(a)).

$$O_2 \xrightarrow{h\nu} 2O^{\bullet} \quad (6)$$

$$O^{\bullet} + O_2 \rightarrow O_3 \quad (7)$$

$$\text{organic residuals} + O_3 \rightarrow \text{–M–O–M–} + CO_2 + H_2O \quad (8)$$

To demonstrate the effective acceleration of the crystallization process of metal oxide thin films using this low-temperature strategy assisted by •OH free radicals, we have chosen as a proof-of-concept the $BiFeO_3$ perovskite system that has a wide range of properties of interest in high-performance multiple-operation devices.[14,38,40] The full process was monitored by Infrared Reflection Absorption Spectroscopy (IRRAS) and Angle-Resolved X-ray Photoemission Spectroscopy (ARXPS) techniques (Fig. S4 and S5, ESI† respectively), showing the corresponding results in Fig. 2.

Fig. 2(a) shows the IRRAS experimental spectra of the films obtained after the different steps of the fabrication process. The first reflectance ratio spectrum of the deposited layer (step 1) presents several modes in the region around 600 $cm^{-1}$ corresponding to different types of metal–oxygen bonds. For wavelengths above 1000 $cm^{-1}$, vibrational modes associated with C–N, RCOO–, N–H, C–H and O–H bonds are observed. All the former signals are ascribed to the different organic species initially present in the system (*i.e.*, metal precursors and organic solvents). At step 2, it can be observed how the O–H signal in the film increases with UV-irradiation at 172 nm under the •OH atmosphere. These free radicals react with the solution-deposited layer producing the rapid formation of M–OH bonds in the film (nucleophilic substitution). The reaction is accompanied by the rupture of the chemical bonds of the organic species contained in the film, which results in an abrupt decrease of the C–H signal. Thus, around 70% more O–H bonds than those of the just deposited film (step 1) are detected at this step 2, whereas the bands ascribed to the C–H bonds practically disappear (Fig. S6a, ESI†). Complementary, bands at ~2341 $cm^{-1}$ and ~2180 $cm^{-1}$ are respectively observed at steps 2 and 3 due to physisorbed $CO_2$ and $NO_x$ at the film surface, which correspond to gas volatile byproducts resulting from the elimination of remnant organics.

At step 4, the bands associated with the transverse stretching M–O bonds have evolved from multiple minima in the deposited layer (*e.g.*, ~510 $cm^{-1}$, ~570 $cm^{-1}$ or ~635 $cm^{-1}$) to a single and more pronounced band (centered at ~630 $cm^{-1}$) in the annealed film. This strong minimum is probably due to the formation of a metal–oxygen structure, where both Bi and Fe atoms participate in a complex oxide with an incipient crystallinity.[45] The contribution of the heavy Bi atoms would shift the vibration frequency of the Fe–O octahedra to the observed value (~630 $cm^{-1}$), considering that the longitudinal mode of the Fe–O octahedra should be close to that of α-$Fe_2O_3$ (located at 662 $cm^{-1}$).[46] Therefore, we can conclude that the film treated at only 350 °C for a short time of 10 min (step 4) displays a structure with an arrangement of the Bi, Fe and O atoms close to that of a cubic $BiFeO_3$ perovskite. Increasing the time of this treatment is sufficient to convert this nanocrystalline oxide film into the final perovskite system. This results in the splitting of the band recorded at ~630 $cm^{11}$ into two minima at ~470 $cm^{-1}$ and ~610 $cm^{-1}$, which are ascribed to the respective high frequency E and $A_1$ modes of the rhombohedral $BiFeO_3$ perovskite (*i.e.*, the fingerprint of the $BiFeO_3$ perovskite).[47] The special configuration of the IRRAS technique allowed us to calculate the phonon frequencies of this $BiFeO_3$ layer, by simulating a spectrum for a ~70 nm thick film that fits well with the experimental one (see Fig. 2(a)).[48,49]

The comparison of the IRRAS spectra of the former films with those of the films processed without •OH radicals (Fig. 2(b) and Fig. S7, ESI†) demonstrates the accelerated crystallization of the $BiFeO_3$ perovskite film assisted by •OH

 

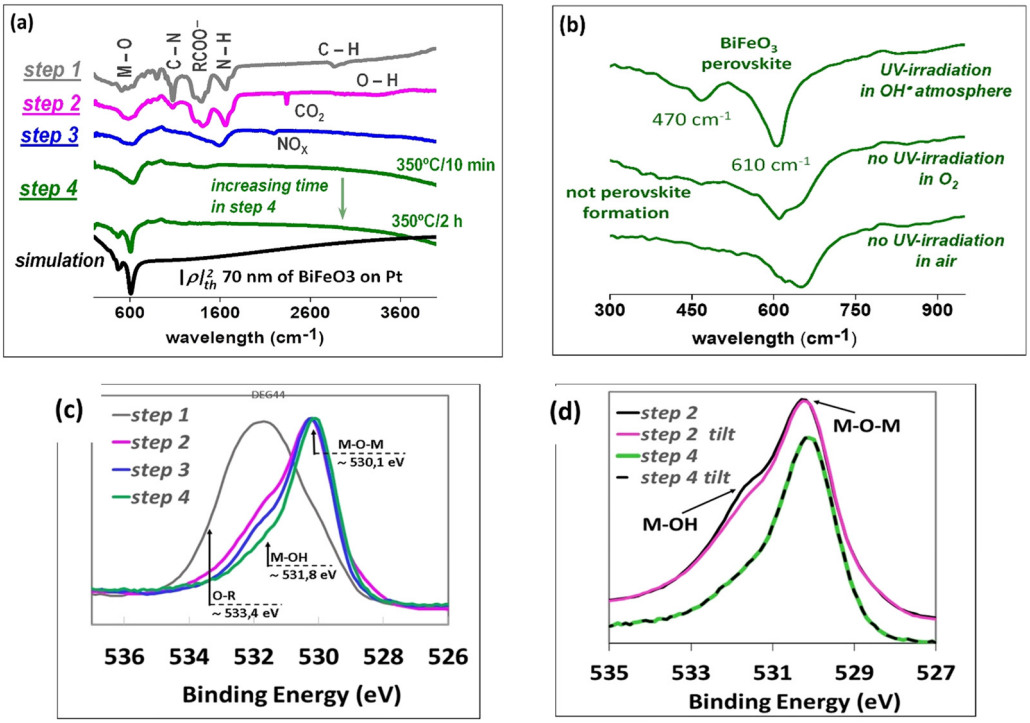


Fig. 2 Effect of the steps of the UV-irradiation process assisted with •OH free radicals on the accelerated crystallization of $BiFeO_3$ perovskite thin films. (a) IRRAS spectra recorded between 200 $cm^{-1}$ and 4000 $cm^{-1}$ for the films obtained after the different steps of the low-temperature solution process. For comparison, the calculated Fourier-transform infrared spectroscopy (FTIR) spectrum of the $BiFeO_3$ perovskite is shown at the bottom of the figure. (b) IRRAS spectra in the region of the M–O bonds recorded for the former films, after the step 4 with a treatment at 350 °C for 2 h and those films obtained in the same way, but without illumination with UV-light in $H_2O$ and $O_2$ atmospheres, and without illumination with UV-light in air atmospheres (see Fig. S3, ESI†). (c) O1s core level ARXPS spectra of the films recorded at 40° take-off angle for the steps 1 to 4 of the process. (d) Comparison of the O1s core level spectra recorded at 40° and 90° take-off angles for the steps 2 and 4 of the process. The intensity of these O1s spectra have been normalized for comparison purposes.

free radicals. These results show an efficient formation of the gel film when it is accelerated by the •OH free radicals generated *in situ* in the irradiation atmosphere (reactions (4) and (5)). On the contrary, the films treated under a water vapor atmosphere without UV-irradiation (Fig. S6b, ESI†) showed a much lower formation rate of the amorphous gel oxide, although it was significantly higher than that of the films only treated in air without UV-irradiation (Fig. S6c, ESI†).[8,25,50,51]

Fig. 2(c) shows the O1s core level spectra recorded by ARXPS with a take-off angle of 40° for the films obtained after the successive steps of the process. The solution-deposited layer (step 1) shows a broad O1s spectrum (FWHM ~ 3.3 eV) with a maximum at ~531.8 eV. This signal can be deconvoluted into three contributions corresponding to oxygen bonded to metals (M–O–M), oxygen from hydroxide groups bonded to metals (M–OH bonds), and oxygen bonded to organic compounds (O–R),[52] from low to high binding energy, respectively (see Fig. S5b, ESI†). At step 2, the broadening of the O1s peak decreases and shifts towards lower binding energies. A maximum at ~530.1 eV ascribed to oxygen bonded to metals (M–O–M), with a shoulder at higher energies due to oxygen in M–OH bonds (reaction (4)), is now observed. At step 3, the intensity of the M–OH shoulder compared to that of the main M–O–M peak is reduced, indicating that an accelerated condensation of the film is in progress (reaction (5)) to form the metal–oxygen network that finally occurs at step 4. Here, the asymmetric shape of the O1s spectrum cannot be related to the contribution of oxygen in M–OH bonds, but to the formation of the $BiFeO_3$ oxide as previously reported for other oxides containing two metal cations arranged into a short-range ordered structure.[53,54] This would be the case of Bi and Fe ions participating in a $BiFeO_3$ film with an incipient crystallinity, as previously demonstrated from the IRRAS results of Fig. 2(a).

Fig. 2(d) shows the O1s core level spectra of the films after the steps 2 and 4 recorded at 40° and 90° take-off angles. Note that, whereas the normal configuration at 90° provides data from the bulk film, information from the film surface is obtained with a tilt angle of 40°. The evolution of the oxygen signal attributed to the M–OH and M–O–M bonds suggests that an oxyhydroxide layer is formed at the step 2 as a result of the attack of the •OH radicals generated within the irradiation atmosphere to the film surface. The reduction of the M–OH shoulder in the spectrum recorded at 40° reveals that this reaction starts in a controlled way from the top surface to the inner layers of the sample. On the other hand, the shape of the O1s peak of the film after the step 4 does not depend on the take-off angle. This supports a gradual and controlled transformation of the solution deposited layer into the final metal

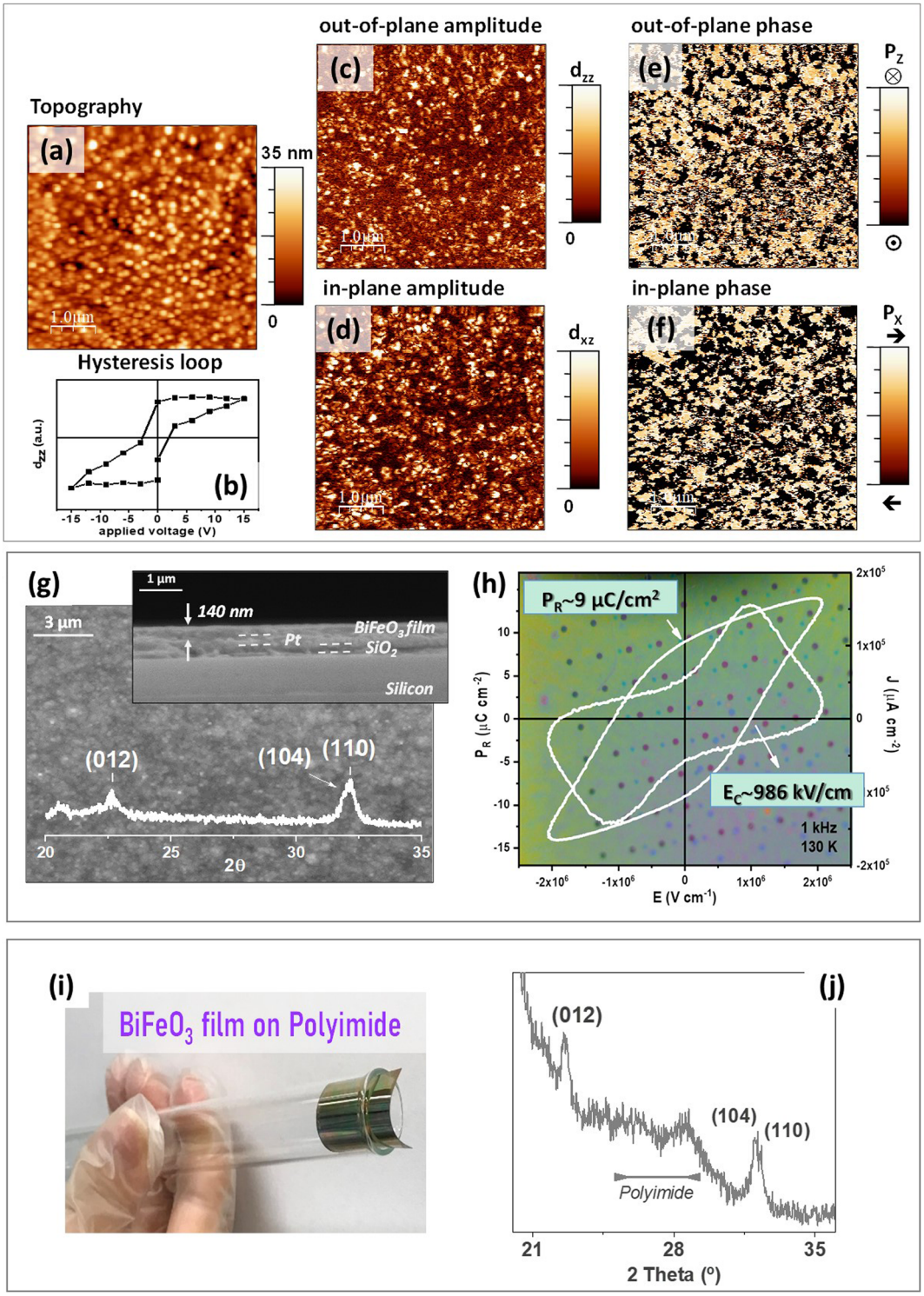


Fig. 3 Demonstration of the functionality of the crystalline $BiFeO_3$ perovskite films obtained by this method at a low temperature of 350 °C for times over 2 h. Crystal structure, microstructure and electrical properties at the nano and macroscale are shown. (a) Topography, (b) local piezoelectric hysteresis loop, (c) and (d) out-of-plane and in-plane amplitude images, and (e), (f) out-of-plane and in-plane phase images, of the $BiFeO_3$ thin films obtained after both UV-irradiation steps (step 2 in •OH atmosphere and step 3 in $O_3$ atmosphere), and a thermal treatment at 350 °C in the step 4. (g) Photograph of the array of capacitor devices fabricated for the electrical characterization and ferroelectric hysteresis loop measured in the former film. (h) Plan-view and cross-section FEGSEM images, and X-ray diffraction pattern of the $BiFeO_3$ thin films prepared on Pt-coated silicon substrates. (i) Photograph of the $BiFeO_3$ film directly processed on a polyimide substrate. (j) X-ray diffraction pattern measured in this film on polyimide. The reflections of the $BiFeO_3$ perovskite have been indexed with the JCPDS-ICDD card no. 01-86-1518.

 

oxide film from top to bottom, indicating the complete formation of a metal–oxygen structure in the system after this step.

To fully demonstrate the functionallity of the crystalline $BiFeO_3$ perovskite films obtained by this method at only 350 °C, capacitor devices were fabricated with thin films grown up to an average thickness of ~140 nm. The low-magnification topographic, and amplitude and phase piezoelectric images obtained by Piezoresponse Force Microscopy (PFM) show a film formed by equiaxial nanometric grains with a piezoelectric response homogeneously distributed over the surface (Fig. 3(a), (c)–(f), and Fig. S8a–e, ESI†). The piezoelectric behavior of this film is additionally confirmed by the hysteresis loop depicted in Fig. 3(b). The plan-view and cross-section FEGSEM images, together with the X-ray diffraction patterns of these films (Fig. 3(g)), denote a nanometric grain size typically obtained in polycrystalline metal oxide films processed at low temperatures. This intrinsic effect, together with the possible existence of residual areas with an incipient crystallinity, is responsible for the characteristic depletion observed in the functional properties of these metal oxide films compared to film counterparts processed at conventional temperatures (≥500 °C).[55] Thus, macroscopic ferroelectric measurements were carried out in the $BiFeO_3$ thin film capacitor devices shown in the photograph of Fig. 3(h). The high quality of the sample is inferred from the fact that around the 95% of the capacitors display high permittivities and low dielectric losses. A representative ferroelectric hysteresis loop measured in these capacitors is inserted in this figure, which clearly demonstrates the ferroelectric response of the films crystallized at 350 °C. A remnant polarization of ~9 μC $cm^{-1}$ is obtained, which fulfills the requirements demanded for the operation of ferroelectric thin films in electronic devices.[14,55,56] When the step 3 is skipped in the fabrication process (only a single UV-irradiation in the $^{\bullet}OH$ atmosphere is just carried out at step 2), the resulting thin-film devices do not show an appropriate performance (Fig. S8h, ESI†). Although the $BiFeO_3$ perovskite is detected in both films (with and without step 3) with similar crystal structure characteristics (as detected by the X-ray diffraction patterns inserted in Fig. S8f–g, ESI†), they present very different ferroelectric behaviour. Note that the densification of the film without the step 3 is lower than that of the film prepared following the complete process. This can be deduced from its thickness, which is around 18% thicker with respect to the film subjected to the complete process (165 nm *versus* 140 nm) (Fig. S8f and g, ESI†). In addition, most of the capacitor devices fabricated in this film are short-circuited (~65%), with the rest of the capacitors showing an inhomogeneous response depicted by ferroelectric hysteresis loops with a large amount of non-switching contributions (leakage currents and conduction). However, a further UV-irradiation of the film in a strong $O_3$ oxidizing atmosphere (step 3) increases the film densification and produces the elimination of defects (porosity, carbonaceous residuals or oxygen vacancies) (reaction (8)).[33,34,57,58] We selected to carry out this step 3 with UV-irradiation at 222 nm because, in the particular case of the precursor solutions used in this work, this emission wavelength is close to the absorption maxima of the metal complexes of the system (Fig. S1, ESI†). Thus, under these conditions the step 3 results very efficient in accelerating not only the oxidation of the organic residuals still present in the film by ozonolysis, but also in promoting the total photolysis of the M–L bonds and the further decomposition of these compounds.

Finally, the low-temperature strategy proposed in this work opens the door to the direct growth of these films on temperature-sensitive substrates like those used in emerging technologies, like those based on flexible electronics. This fact is demonstrated by the fabrication of $BiFeO_3$ thin films on flexible polyimide substrates (Fig. 3(i)). The X-ray diffraction pattern of these films (Fig. 3(j)) shows the reflections corresponding to the perovskite phase together with the characteristic diffuse background of the polymeric compound. Besides being transferible to different types of substrates, the solution process developed here can also be extended to any other metal oxide composition requiring a crystalline degree to reach an adequate performance. This is confirmed by the low-temperature processing at 350 °C of both rigid and flexible thin films of the model ferro-piezoelectric $Pb(Zr_{0.30}Ti_{0.70})O_3$ (PZT) perovskite oxide. The quality of these films is shown by their well-defined ferroelectric response with values of remnant polarization of ~14 μC $cm^{-1}$ (Fig. S9a–e, ESI†). It must be highlighted that the crystallization of a binary oxide should occur more easily (*i.e.*, under a lower thermal budget) compared to a multiple oxide. Thus, crystalline $Bi_2O_3$ thin films were also obtained by this method after applying a heating treatment of only 250 °C (Fig. S9f, ESI†). The demostration that the crystallization of metal oxide thin films can be effectively accelerated by $^{\bullet}OH$ radicals generated *in situ* during the UV-irradiation of solution-deposited layers brings new and exciting opportunities of application for these functional materials. The fabrication process shown in this work enables a significant reduction of the processing temperature, which results in a low energy consumption and carbon footprint as main benefits. Furthermore, we validate here the general application of this solution deposition method for the fabrication of thin films of any metal oxide directly on temperature-sensitive substrates, which is a key requirement for the next-generation high-performance and flexible devices demanded today by the emerging technologies.

## 3. Conclusion

A novel photochemical strategy is proposed in this work for accelerating the crystallization of metal oxide thin films. The UV-irradiation of solution-deposited layers in the presence of water vapor is shown to generate hydroxyl radicals ($^{\bullet}OH$) in the reaction atmosphere that play a fundamental role in the formation of the oxide. These species attack the surface of the film promoting the nucleophilic substitution of the alkoxy groups (–OR), constituent of the metal precursors, and the polycondensation among them. As a result, the elimination of organic compounds from the system and the subsequent formation of an amorphous metal–oxygen network are significantly boosted at very low temperatures (150 °C). Further UV-irradiation in

ozone atmosphere contributes to enhance thin film densification and to compensate lattice defects (oxygen vacancies) during the early stages of crystallization of the corresponding metal oxide at temperatures just between 250–350 °C. Besides being validated for several crystalline compositions (*e.g.*, $BiFeO_3$, $PbZr_{0.3}Ti_{0.7}O_3$, $Bi_2O_3$), the reported method allows the direct growth of multifunctional oxide layers on flexible and low-cost polymeric substrates, demonstrating adequate device performance for applications in digital technology (*e.g.* ferroelectric memories or piezoelectric actuators). Thus, the accelerated crystallization of metal oxide thin films assisted by hydroxyl radicals at such low temperatures provides stimulating prospects in the fabrication of next-generation eletronic systems basing on a highly versatile solution method with a reduced energy consumption and a decreased carbon footprint.

# 4. Experimental section

### Synthesis of photosensitive solutions

Fig. S1 (ESI†) shows the flow charts corresponding to the synthesis of the precursor solutions which were synthesized accordingly to procedures reported elsewhere.[34–36]

### Thin film deposition, UV-irradiation and annealing processes

Layers from the precursor solutions were deposited on rigid $Pt/TiO_2/SiO_2/(100)Si$ (Radiant Technologies Inc.) and flexible Pt/NiCr/PI/NiCr/Pt (75 μm thick UPILEX-S polyimide – PI, UBE Industries Ltd) substrates by spin-coating (2000 rpm for 45 s) or dip-coating (drawl speed of 150 mm $min^{-1}$). The solution layers were dried at 150 °C for 5 min on a hot-plate. Then, the films were UV-irradiated in two-laboratory-scale reactors with high-intensity excimer lamps of $\lambda$ of 172 nm (heating at 150 °C/30 min) and 222 nm (heating at 150 °C/30 min and 250 °C/30 min), and under irradiation atmospheres of $H_2O$ and $O_2$, respectively (Fig. S2, ESI†). The irradiated films were then annealed at low temperatures in a Rapid Thermal Processor (JIPELEC JetStar 100T), using a heating rate of ~3 °C $s^{-1}$ and an oxygen atmosphere. The RTP treatment was depending on the complexity of the oxide. For the binary $Bi_2O_3$ films, treatments between 250 °C and 350 °C with soaking times of 10 min were applied. For the complex oxide films of the $BiFeO_3$ and PZT perovskites, treatments at 350 °C with soaking times between 10 min and 10 h were applied. The temperature of the RTP treatment was monitored not only with the internal controllers of the equipment (thermocouple and pyrometer), but also with an external thermocouple located on the film surface. For the flexible films, these treatments were made using special home-built sample holders.[41] To demonstrate the efficiency of the UV-irradiation, similar films were deposited from the same solutions and subjected to the same processes but without UV-irradiation, under the same atmospheres and in air (Fig. S3, ESI†).

### Infrared reflection absorption spectroscopy (IRRAS) analysis

IRRAS experimental measurements were performed in a Bruker IFS 66V-S, on the films deposited on $Pt/TiO_2/SiO_2/(100)Si$ with thickness below 100 nm. Fig. S4 (ESI†) shows a scheme of the configuration of the IRRAS technique used for the characterization of the films.

### Angle resolved X-ray photoelectron spectroscopy (ARXPS) analysis

ARXPS measurements have been performed with a Mg Kα X-ray source, $h\nu$ = 1253.6 eV, an analyzer pass energy of 20 eV and a micrometric manipulator, $XYZ\theta$ (for the sample positioning and tilting). Take-off angles of 40° and 90° with respect to the hemispherical analyzer were used (Fig. S5, ESI†). The use of the ARXPS technique for the study of the films of this work avoids the modification produced in the samples when argon ion bombardment is used to obtain depth profiles.

### Crystal structure and microstructure

The crystallinity of the films was followed by X-ray diffraction (D8 ADVANCE instrument, Cu Kα radiation, Bruker), using a Bragg–Brentano geometry and a wavelength of the incident beam of $\lambda_{CuK\alpha}$ = 1.5418 Å. Scanning electron microscopy was used to observe the surface morphology of the thin films (Nova NanoSEM 230 instrument, FEI Company).

### Ferroelectric and piezoelectric characterization

These measurements were carried out on the $BiFeO_3$ and PZT thin films grown on rigid $Pt/TiO_2/SiO_2/(100)Si$ and flexible Pt/NiCr/PI/NiCr/Pt substrates up to thicknesses between 100 nm and 200 nm. The final crystallization of these films was carried out at 350 °C with soaking times between 2 h and 10 h. Ferroelectric hysteresis loops were measured under sinusoidal excitation (2–100 V amplitude, 0.1–20 kHz frequency) using a virtual ground system composed by a pulse generator (33220A Arbitrary Waveform Generator, Agilent), a power amplifier (High-Voltage Amplifier 9100, Tabor Electronics), a current amplifier (428-PROG Programmable Current Amplifier, Keithley), and an oscilloscope (TDS 520, Tektronix). Planar arrays of capacitors were fabricated by the evaporation of top Pt electrodes on the film surface through a shadow mask (diameter of ~100 μm and ~200 μm and thickness of ~10 nm). Charge loops were obtained by numerical integration from the respective current loops. Topography and Piezoresponse Force Microscopy (PFM) images of the film surfaces were obtained with a scanning force microscopy (Nanotec® with WSxM® software). PFM measurements were obtained with AC voltages of 3.5 V of amplitude at 50 kHz, using conductive Pt/Ir-coated tips on cantilevers with 42 N $m^{-1}$ (PPP-NCHPt probes, Nanosensors).

# Author contributions

MLC and IB conceived the study, wrote the paper, performed the fabrication of the films and their crystal structure and microstructural characterization. AGL and YAR participated in the fabrication and characterization of the films. RJ carried out the dielectric and ferroelectric characterization of the films, evaluating their functionality for applications. JR and SLF

 

studied the crystalline films by AFM and PFM. CP performed the IRRAS experiments and analyzed these results. IM performed the ARXPS experiments and analyzed these results. All the authors contribute to the final version of this paper.

## Conflicts of interest

There are no conflicts to declare.

## Acknowledgements

This work is part of the Spanish Project PID2019-104732RB-I00 funded by MCIN/AEI/10.13039/501100011033. I. B. acknowledges Grant RYC-2016-20047 funded by MCIN/AEI/10.13039/501100011033. A. Y. R. and S. L. acknowledge the financial support of CAM, PEJ-2019-AI/IND-13396 and PEJ-2020-AI/IND-18134.

## References

1 S. Park, C.-H. Kim, W.-J. Lee, S. Sung and M.-H. Yoon, Sol–gel metal oxide dielectrics for all-solution-processed electronics, *Mater. Sci. Eng., R*, 2017, **114**, 1–22.
2 J. W. Park, B. H. Kang and H. J. Kim, A Review of Low-Temperature Solution-Processed Metal Oxide Thin-Film Transistors for Flexible Electronics, *Adv. Funct. Mater.*, 2020, **30**, 1904632.
3 M. L. Calzada, Sol–Gel Electroceramic Thin Films, in *The Sol–Gel Handbook: Synthesis Characterization*, ed. D. Levy, M. Zayat, Wiley-VCH, Weinheim, 2015, vol. 2, ch. 27.
4 I. Bretos, R. Jiménez, J. Ricote and M. L. Calzada, Low-temperature crystallization of solution-derived metal oxide thin films assisted by chemical processes, *Chem. Soc. Rev.*, 2018, **47**, 291–308.
5 L. Song, S. Glinsek and E. Defay, Toward low-temperature processing of lead zirconate titanate thin films: Advances, strategies, and applications, *Appl. Phys. Rev.*, 2021, **8**, 041315.
6 F. An, M. Zi, Q. Chen, C. Liu, K. Qu, T. Jia, M. Huang and G. Zhong, Flexible room-temperature multiferroic thin film with multifield tunable coupling properties, *Mater. Today Phys.*, 2022, **23**, 100615.
7 T. Nakajima, Y. Fujio, T. Sugahara and T. Tsuchiya, Flexible Ceramic Film Sensors for Free-Form Devices, *Sensors*, 2022, **22**, 1996.
8 K. K. Banger, Y. Yamashita, K. Mori, R. L. Peterson, T. Leedham, J. Rickard and H. Sirringhaus, Low-temperature, high-performance solution-processed metal oxide thin-film transistors formed by a 'sol–gel on chip' process, *Nat. Mater.*, 2011, **10**(1), 45–50.
9 S. Park, K.-H. Kim, J.-W. Jo, S. Sung, K.-T. Kim, W.-J. Lee, J. Kim, H. J. Kim, G.-R. Yi, Y.-H. Kim and M.-H. Yoon, S. K. Park. In-Depth Studies on Rapid Photochemical Activation of Various Sol–Gel Metal Oxide Films for Flexible Transparent Electronics, *Adv. Funct. Mater.*, 2015, **25**, 2807–2815.
10 S. Lee, S. H. Lee, N. On and J. K. Jeong., A solution-processed La–Zr–O dielectric at a low temperature for high-performance In-Ga-O transistors: Engineering a precursor solution, *Ceram. Int.*, 2021, **47**, 6918–6927.
11 M.-H. Jao, C.-C. Cheng, C.-F. Lu, K.-C. Hsiao and W.-F. Su, Low temperature and rapid formation of high quality metal oxide thin film *via* a hydroxide assisted energy conservation strategy, *J. Mater. Chem. C*, 2018, **6**, 9941–9949.
12 G. Feng, P. Cheng, W. Yan, M. Boronat, X. Li, J.-H. Su, J. Wang, Y. Li, A. Corma, R. Xu and J. Yu, Accelerated crystallization of zeolites *via* hydroxyl free radicals, *Science*, 2016, **351**, 62781188.
13 I. Bretos, R. Jiménez, J. Ricote and M. L. Calzada, Photochemistry in the Low-Temperature Processing of Metal Oxide Thin Films by Solution Methods, *Chem. – Eur. J.*, 2020, **26**, 9277–9291.
14 I. Bretos, R. Jiménez, J. Ricote and M. L. Calzada, Low-Temperature Solution Approaches for the Potential Integration of Ferroelectric Oxide Films in Flexible Electronics, *IEEE Trans. Ultrason. Eng.*, 2020, **67**(10), 1967–1979.
15 J. T. Anderson, C. L. Munsee, C. M. Hung, T. M. Phung, G. S. Herman, D. C. Johnson, J. F. Wager and D. A. Keszler, Solution-processed HafSOx and ZircSOx inorganic thin-film dielectrics and nanolaminates, *Adv. Funct. Mater.*, 2007, **17**, 2117–2124.
16 S. T. Meyers, J. T. Anderson, D. Hong, C. M. Hung, J. F. Wager and D. A. Keszler, Solution-processed aluminum oxide phosphate thin-film dielectrics, *Chem. Mater.*, 2007, **19**, 4023–4029.
17 K. M. Kim, C. W. Kim, J.-S. Heo, H. Na, J. E. Lee, C. B. Park, J.-U. Bae, C.-D. Kim, M. Jun, Y. K. Hwang, S. T. Meyers, A. Grenville and D. A. Keszler, Competitive device performance of low-temperature and all-solution-processed metal-oxide thin-film transistors, *Appl. Phys. Lett.*, 2011, **99**, 242109.
18 J.-B. Seon, S. Lee, J. M. Kim and H.-D. Jeong, Spin-Coated CdS Thin Films for n-Channel Thin Film Transistors, *Chem. Mater.*, 2009, **21**, 604–611.
19 K. Jiang, J. T. Anderson, K. Hoshino, D. Li, J. F. Wager and D. A. Keszler, Low-Energy Path to Dense $HfO_2$ Thin Films with Aqueous Precursor, *Chem. Mater.*, 2011, **23**, 945–952.
20 Y. C. Zhang, G. He, L. N. Wang, W. H. Wang, X. F. Xu and W. J. Liu, Ultraviolet-Assisted Low-Thermal-Budget-Driven alpha-InGaZnO Thin Films for High-Performance Transistors and Logic Circuits, *ACS Nano*, 2022, **16**(3), 4961–4971.
21 W. Yang, K. Song, Y. Jung, S. Jeong and J. Moon, Solution-deposited Zr-doped AlOx gate dielectrics enabling high-performance flexible transparent thin film transistors, *J. Mater. Chem. C*, 2013, **1**, 4275–4282.
22 J. H. Park, K. Kim, Y. B. Yoo, S. Y. Park, K.-H. Lim, K. H. Lee, H. K. Baik and Y. S. Kim, Water adsorption effects of nitrate ion coordinated $Al_2O_3$ dielectric for high performance metal-oxide thin-film transistor, *J. Mater. Chem. C*, 2013, **1**, 7166–7174.
23 J. H. Park, Y. B. Yoo, K. H. Lee, W. S. Jang, J. Y. Oh, S. S. Chae and H. K. Baik, Low-Temperature, High-Performance Solution-Processed Thin-Film Transistors with Peroxo-Zirconium Oxide Dielectric, *ACS Appl. Mater. Interfaces*, 2012, **5**, 410–417.

24 J. H. Park, S. J. Lee, T. I. Lee, J. H. Kim, C.-H. Kim, G. S. Chae, M.-H. Ham, H. K. Baik and J.-M. Myoung, All-solution-processed, transparent thin-film transistors based on metal oxides and single-walled carbon nanotubes, *J. Mater. Chem. C*, 2013, **1**, 1840–1845.

25 K. Jiang, S. T. Meyers, M. D. Anderson, D. C. Johnson and D. A. Keszler, Functional Ultrathin Films and Nanolaminates from Aqueous Solutions, *Chem. Mater.*, 2013, **25**, 210–214.

26 S. Choi, B.-Y. Park and H.-K. Jung, Growth and characterization of sol–gel prepared $Gd_2O_3$ films as gate insulators for Zn–Sn–O thin film transistors, *Thin Solid Films*, 2013, **534**, 291–295.

27 Y. S. Rim, H. Chen, X. Kou, H.-S. Duan, H. Zhou, M. Cai, H. J. Kim and Y. Yang, Boost Up Mobility of Solution-Processed Metal Oxide Thin-Film Transistors *via* Confining Structure on Electron Pathways, *Adv. Mater.*, 2014, **26**(25), 4273–4278.

28 W. Xu, H. Wang, F. Xie, J. Chen, H. Cao and J.-B. Xu, Facile and Environmentally Friendly Solution-Processed Aluminum Oxide Dielectric for Low-Temperature, High-Performance Oxide Thin-Film Transistors, *ACS Appl. Mater. Interfaces*, 2015, **7**, 5803–5810.

29 J. Chung, Y. J. Tak, W. G. Kim, J. W. Park, T. S. Kim, J. H. Lim and H. J. Kim., Low-temperature fabrication of solution-processed hafnium oxide gate insulator films using a thermally purified solution process, *J. Mater. Chem. C*, 2018, **6**, 4928–4935.

30 J. Kim, M. Kim, Y. Kang, K.-T. Kim, J.-S. Heo, S. K. Park and Y.-H. Kim, Photoactivated high-*k* lanthanum oxide-aluminum oxide ($La_2O_3$e$Al_2O_3$) alloy-type gate dielectrics for low-voltage-operating flexible transistors, *J. Alloys Compd.*, 2020, **842**, 155671.

31 M. Mandeljc, M. Kosec, B. Malic and Z. Samardzija, Low temperature processing of lanthanum doped PZT thin films, *Integr. Ferroelectr.*, 2000, **30**(1–4), 149–156.

32 M. Kosec, B. Malic and M. Mandeljc, Chemical solution deposition of PZT thin films for microelectronics, *Mater. Sci. Semicond. Process.*, 2002, **5**(2–3), 97–103.

33 M. Calzada, I. Bretos, R. Jimenez, H. Guillon and L. Pardo, Low-temperature processing of ferroelectric thin films compatible with silicon integrated circuit technology, *Adv. Mater.*, 2004, **16**(18), 1620–1624.

34 N. Martín-Arbella, I. Bretos, R. Jiménez, M. L. Calzada and R. Sirera, Photoactivation of Sol–Gel Precursors for the Low-Temperature Preparation of $PbTiO_3$ Ferroelectric Thin Films, *J. Am. Ceram. Soc.*, 2011, **94**(2), 396–403.

35 D. Pérez-Mezcua, R. Sirera, R. Jimenez, I. Bretos, C. De Dobbelaere, A. Hardy, M. K. Van Bael and M. L. Calzada, A UV-absorber bismuth(III)-*N*-methyldiethanolamine complex as a low-temperature precursor for bismuth-based oxide thin films, *J. Mater. Chem. C*, 2014, **2**(41), 8750–8760.

36 I. Bretos, R. Jiménez, A. Wu, A. I. Kingon, P. M. Vilarinho and M. L. Calzada, Activated Solutions Enabling Low-Temperature Processing of Functional Ferroelectric Oxides for Flexible Electronic, *Adv. Mater.*, 2014, **26**(9), 1405–1409.

37 E. K. Michael-Sapia, H. U. Li, T. N. Jackson and S. Trolier-McKinstry, Nanocomposite bismuth zinc niobate tantalate for flexible energy storage applications, *J. Appl. Phys.*, 2015, **118**(23), 234102.

38 M. Tomczyk, I. Bretos, R. Jimenez, A. Mahajan, E. V. Ramana, M. L. Calzada and P. M. Vilarinho, Direct fabrication of $BiFeO_3$ thin films on polyimide substrates for flexible electronics, *J. Mater. Chem. C*, 2017, **5**(47), 12529–12537.

39 I. Bretos, R. Jiménez, D. Pérez-Mezcua, N. Salazar, J. Ricote and M. L. Calzada, Low-Temperature Liquid Precursors of Crystalline Metal Oxides Assisted by Heterogeneous Photocatalysis, *Adv. Mater.*, 2015, **27**(16), 2608–2613.

40 I. Bretos, R. Jimenez, J. Ricote, R. Sirera and M. L. Calzada, Photoferroelectric Thin Films for Flexible Systems by a Three-in-One Solution-Based Approach, *Adv. Funct. Mater.*, 2020, **30**(32), 2001897.

41 O. Barrios, R. Jiménez, J. Ricote, P. Tartaj, M. L. Calzada and I. Bretos, A Sustainable Self-Induced Solution Seeding Approach for Multipurpose $BiFeO_3$ Active Layers in Flexible Electronic Devices, *Adv. Funct. Mater.*, 2022, **32**(27), 2112944.

42 P. T. Tue, T. Shimoda and Y. Takamura, A facile solution-combustion-synthetic approach enabling low-temperature PZT thin-films, *APL Mater.*, 2020, **8**, 021112.

43 S. Z. Zard, *Radical Reactions in Organic Synthesis*, Oxford Univ. Press, London, UK, 2003.

44 G. Moad and D. H. Solomon, *The Chemistry of Radical Polymerization. Elsevier*, Amsterdam, The Netherlands, 2006.

45 K. Bakken, V. H. Pedersen, A. B. Blichfeld, I.-E. Nylund, S. Tominaka, K. Ohara, T. Grande and M.-A. Einarsrud, Structures and Role of the Intermediate Phases on the Crystallization of BaTiO3 from an Aqueous Synthesis Route, *ACS Omega*, 2021, **6**, 9567–9576.

46 S. Onari, T. Arai and K. Kudo, IR lattice-vibrations and dielectric-dispersion in alpha-$Fe_2O_3$, *Phys. Rev. B: Solid State*, 1977, **16**(4), 1717–1721.

47 P. Hermet, M. Goffinet, J. Kreisel and P. Ghosez, Raman and infrared spectra of multiferroic bismuth ferrite from first principles, *Phys. Rev. B: Condens. Matter Mater. Phys.*, 2007, **75**, 220102(R).

48 S. Kamba, D. Nuzhnyy, M. Savinov, J. Šebek, J. Petzelt, J. Prokleška, R. Haumont and J. Kreisel, Infrared and terahertz studies of polar phonons and magnetodielectric effect in multiferroic $BiFeO_3$ ceramics, *Phys. Rev. B: Condens. Matter Mater. Phys.*, 2007, **75**, 024403.

49 R. P. S. M. Lobo, R. L. Moreira, D. Lebeugle and D. Colson, Infrared phonon dynamics of a multiferroic $BiFeO_3$ single crystal, *Phys. Rev. B: Condens. Matter Mater. Phys.*, 2007, **76**, 172105.

50 D. Pérez-Mezcua, I. Bretos, R. Jiménez, J. Ricote, R. J. Jiménez-Rioboó, C. Gonçalves da Silva, D. Chateigner, L. Fuentes-Cobas, R. Sirera and M. L. Calzada, Photochemical solution processing of films of metastable phases for flexible devices: the beta-$Bi_2O_3$ polymorph, *Sci. Rep.*, 2016, **6**, 39561.

51 I. Bretos, R. Jimenez, J. Garcia-Lopez, L. Pardo and M. L. Calzada, Photochemical solution deposition of lead-based

 

ferroelectric films: Avoiding the PbO-excess addition at last, *Chem. Mater.*, 2008, **20**(18), 5731–5733.

52 National Institute of Standards and Technology (NIST) X-ray Photoelectron Spectroscopy Database. NIST Standard Reference Database 20, Version 4.1. US.

53 Y.-H. Kim, J.-S. Heo, T.-H. Kim, S. Park, M.-H. Yoon, J. Kim, M. S. Oh, G.-R. Yi, Y.-Y. Noh and S. K. Park, Flexible metal-oxide devices made by room-temperature photochemical activation of sol–gel films, *Nature*, 2012, **489**, 128–191.

54 J. C. Dupin, D. Gonbeau and P. Vinatier, A. Levasseur. Systematic XPS studies of metal oxides, hydroxides and peroxides, *Phys. Chem. Chem. Phys.*, 2000, **2**(6), 1319.

55 C. Gutierrez-Lazaro, I. Bretos, R. Jimenez, J. Ricote, H. El Hosiny, D. Perez-Mezcua, R. J. Jimenez Rioboo, M. Garcıa-Hernandez and M. L. Calzada, Solution Synthesis of $BiFeO_3$ Thin Films onto Silicon Substrates with Ferroelectric, Magnetic, and Optical Functionalities, *J. Am. Ceram. Soc.*, 2013, **96**(10), 3061–3069.

56 C. De Dobbelaere, M. L. Calzada, R. Jimenez, J. Ricote, I. Bretos, J. Mullens, A. Hardy and M. K. Van Bael, Aqueous Solutions for Low-Temperature Photoannealing of Functional Oxide Films: Reaching the 400 degrees C Si-Technology Integration Barrier, *J. Am. Chem. Soc.*, 2011, **133**(33), 12922.

57 A. L. Kholkin, S. O. Iakovlev and J. L. Baptista, Direct effect of illumination on ferroelectric properties of lead zirconate titanate thin films, *Appl. Phys. Lett.*, 2001, **79**, 2055–2057.

58 Y. J. Tak, D. H. Yoon, S. Yoon, U. H. Choi, M. M. Sabri, B. D. Ahn and H. J. Kim, Enhanced Electrical Characteristics and Stability *via* Simultaneous Ultraviolet and Thermal Treatment of Passivated Amorphous In–Ga–Zn–O Thin-Film Transistors, *ACS Appl. Mater. Interfaces*, 2014, **6**(9), 6399–6405.